Supplementary Data (ESI)

A High Nuclearity Mixed Valence {Mn_{32}} Complex

Stuart K. Langley[a], Rachel Stott[a], Nicholas F. Chilton,[a] Boujemaa Moubaraki[a] and Keith S. Murray[*, a]

[a] School of Chemistry, Monash University, Clayton, Victoria 3800, Australia

- **Experimental information for the synthesis of $[Mn^{II}_{18}Mn^{III}_{10}Mn^{IV}_{4}(OH)_{24}O_{14}(OMe)_6(O_2CC(CH_3)_3)_{24}(H_2O)_{2.6}]\cdot 5CH_2Cl_2$ (1).**

$Mn(O_3SC_6H_4CH_3)_2\cdot 6H_2O$ (0.5 g, 1 mmol) was dissolved in 20 ml of MeOH followed by the addition of pivalic acid (0.075 g, 0.75 mmol) and triethylamine (0.14 ml, 1 mmol) to give a deep brown solution. This was then stirred for 15 minutes, after-which the solvent was then removed and re-dissolved CH_2Cl_2. This was then allowed to evaporate slowly and after several days, large brown prismatic crystals of **1** had formed. Yield: 12 mg, 7 %. Anal. Calculated (found) for **1**·$5Cl_2CH_2$: $Mn_{32}C_{131}H_{273.2}O_{94.6}Cl_{10}$: C, 28.79 (28.43); H, 5.03 (4.75); N, 6.49 (6.43). Selected ATR IR data (cm^{-1}): 3417w, 3033s, 1691s, 1588sh, 1567s, 1480s, 1459sh, 1409s, 1372sh, 1357s, 1223w, 1033w, 1009w, 892w.

Elemental analyses (CHN) were carried out by Campbell Microanalytical Laboratory, University of Otago, Dunedin, New Zealand. IR spectra were recorded on a Bruker Equinox 55 spectrometer with an ATR sampler provided by Specac inc. and the samples were run neat.

X-Ray crystallographic measurements were performed at 123(2) K for **1** using a Bruker Smart Apex X8 diffractometer with Mo Kα radiation. The data collection and integration were performed within SMART and SAINT+ software programs, and corrected for absorption using the Bruker SADABS program. Crystallographic data and refinement parameters for **1** are summarized in the notes and reference section of the script.

DC magnetic susceptibility measurements were carried out on a Quantum Design MPMS 5 SQUID magnetometer calibrated by use of a standard palladium sample (Quantum Design) of accurately known magnetization or by use of magnetochemical calibrants such as $CuSO_4 \cdot 5H_2O$. Microcrystalline samples were dispersed in Vaseline in order to avoid torquing of the crystallites. The freshly prepared sample remained crystalline and thus did not lose any solvent of crystallization upon the loading process. The sample mulls were contained in a calibrated gelatine capsule held at the centre of a drinking straw that was fixed at the end of the sample rod. Magnetisation isotherm measurements were made in fields of between 0 and 5 T. AC susceptibilities were made using a Quantum Design PPMS instrument with an AC field of 5 Oe and frequencies varying over the range 20 to 1500 Hz, at temperatures between 2 and 10 K.

Assignment of oxidation states from BVS calculations and coordination sphere considerations.

Atoms	Mn(II)	Mn(III)	Mn(IV)
Mn1	**2.11**	1.94	1.91
Mn2	3.29	**3.13**	3.07
Mn3	3.39	**3.11**	3.07
Mn4	3.28	**3.02**	2.97
Mn5	2.09	1.93	1.89
Mn6	**2.13**	1.97	1.93
Mn7	**2.00**	1.84	1.81
Mn8	**2.35**	2.20	2.16
Mn9	4.20	3.87	**3.80**
Mn10	**2.03**	1.87	1.84
Mn11	4.29	3.95	**3.88**
Mn12	**2.14**	1.97	1.93
Mn13	**1.84**	1.70	1.66
Mn14	2.86	**2.70**	2.66
Mn15	3.60	**3.32**	3.26
Mn16	**2.14**	1.98	1.94

Table S1. Bond valence sum calculations for **1**. The oxidation state for each metal is the whole number closest to the value in bold.

Mn1-O1	2.118(7)	Mn5-O46	2.121(5)	Mn9-O13	1.882(5)	Mn13-O38	2.116(6)
Mn1-O32[1]	2.140(5)	Mn5-O12	2.135(5)	Mn9-O24	1.901(5)	Mn13-O45	2.131(6)

Mn1-O2	2.145(7)	Mn5-O25	2.177(5)	Mn9-O32	1.920(5)	Mn13-O39	2.151(7)
Mn1-O4	2.195(6)	Mn5-O23	2.191(5)	Mn9-O22	1.926(5)	Mn13-O41	2.185(5)
Mn1-O3	2.214(6)	Mn5-O29	2.203(5)	Mn9-O21	1.940(5)	Mn13-O40	2.225(6)
Mn1-O43^{I}	2.270(6)	Mn5-O24	2.263(5)	Mn9-O23	1.964(6)	Mn14-O43	2.004(7)
Mn2-O5	1.918(5)	Mn6-O13	2.126(5)	Mn10-O31^{I}	2.114(7)	Mn14-O44	2.010(6)
Mn2-O33^{I}	1.926(5)	Mn6-O16	2.131(6)	Mn10-O42^{I}	2.119(7)	Mn14-O40	2.030(6)
Mn2-O7	1.977(5)	Mn6-O14	2.144(6)	Mn10-O30	2.169(6)	Mn14-O34	2.072(5)
Mn2-O3	2.031(6)	Mn6-O10	2.173(6)	Mn10-O23	2.200(6)	Mn14-O8^{I}	2.107(6)
Mn2-O6	2.074(5)	Mn6-O8	2.226(5)	Mn10-O29	2.215(5)	Mn14-O41	2.235(6)
Mn2-O43^{I}	2.225(7)	Mn6-O12	2.251(5)	Mn10-O32	2.383(5)	Mn15-O28	1.878(5)
Mn3-O7	1.909(5)	Mn7-O15	2.115(7)	Mn11-O28	1.867(5)	Mn15-O13^{I}	1.891(5)
Mn3-O12	1.928(5)	Mn7-O17	2.138(6)	Mn11-O24	1.901(5)	Mn15-O34	1.984(5)
Mn3-O9	1.929(5)	Mn7-O21	2.178(5)	Mn11-O32	1.906(5)	Mn15-O35	1.994(5)
Mn3-O33^{I}	1.957(5)	Mn7-O35^{I}	2.211(5)	Mn11-O34	1.927(5)	Mn15-O22^{I}	2.067(5)
Mn3-O11	2.193(5)	Mn7-O18	2.248(8)	Mn11-O41	1.943(5)	Mn15-O40	2.119(6)
Mn3-O8	2.207(5)	Mn7-O18’	1.95(2)	Mn11-O29	1.946(5)	Mn16-O22	2.007(5)
Mn4-O6	1.904(5)	Mn8-O19	2.042(6)	Mn12-O36	2.124(6)	Mn16-O33	2.021(5)
Mn4-O11	1.907(5)	Mn8-O22	2.081(5)	Mn12-O37	2.135(6)	Mn16-O34	2.022(5)
Mn4-O25	1.973(5)	Mn8-O3^{I}	2.105(6)	Mn12-O27	2.143(5)	Mn16-O24^{I}	2.035(5)
Mn4-O20^{I}	2.003(5)	Mn8-O35^{I}	2.129(5)	Mn12-O28	2.155(5)		
Mn4-O26	2.120(6)	Mn8-O20	2.183(5)	Mn12-O25	2.234(5)		
Mn4-O33^{I}	2.323(5)	Mn8-O21	2.249(5)	Mn12-O20^{I}	2.258(5)		

Table S2. Selected bond lengths (Å) for complex **1**. Symmetry transformation: (I) 1 - x, 2 - y, 2 - z.

Mn1, Mn6, Mn7, Mn8, Mn10 and Mn12 are all 6 co-ordinate with octahedral geometries. No Jahn-Teller distortions are observed at each coordination site and thus from the BVS calculations and the relatively long bond distances observed, these ions are assigned as (2+). Mn13 is 5 coordinate with a square pyramidal geometry again there is no distortion due to the Jahn-Teller effect and thus from this and BVS calculations we determine this to be (2+). Mn16 is four coordinate with a tetrahedral geometry, BVS calculations and its geometry allows us to assign this ion as (2+).
Mn2, Mn3, Mn4, Mn14 and Mn15 all display Jahn-Teller distorted octahedral co-ordination spheres, with an elongation of the axial bonds with shorter equatorial bonds. This evidence as well as the BVS calculations suggests that these ions are (3+).

Mn9 and Mn11 both display octahedral geometries with no Jahn-Teller distortions and with each bond displaying similar relatively shorter bond lengths. This and the BVS calculations suggest these ions are (4+).

Moreover the assignment of these oxidation states agrees with the charge balance considerations for this complex.

- **Magnetic data on two new freshly prepared samples of 1**

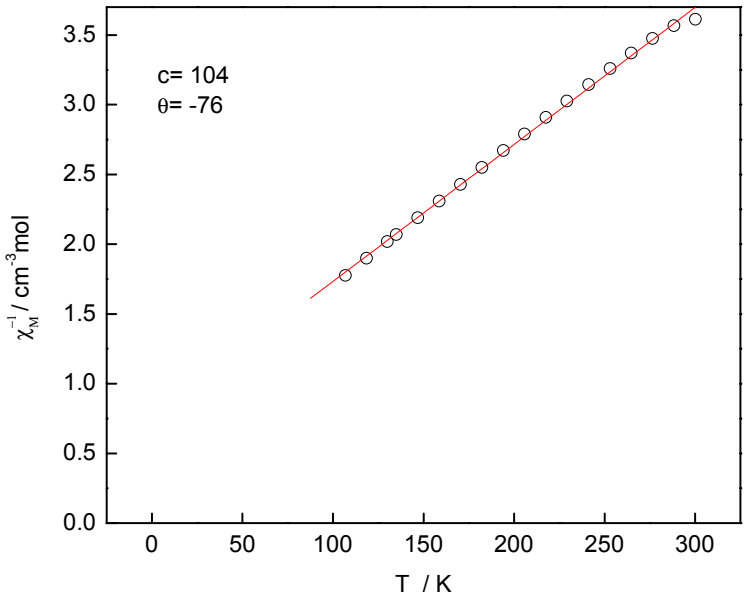

Fig S1. Plot of 1/ χ_M vs *T* from DC data for freshly prepared **1**. (new sample 1)

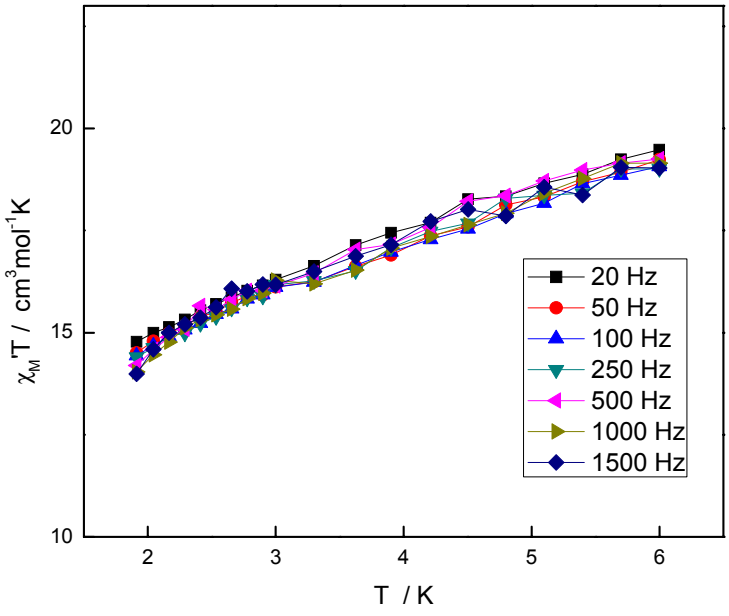

Fig. S2. Plot of AC $\chi_M'T$ *vs. T* for freshly prepared **1**. (new sample 1)

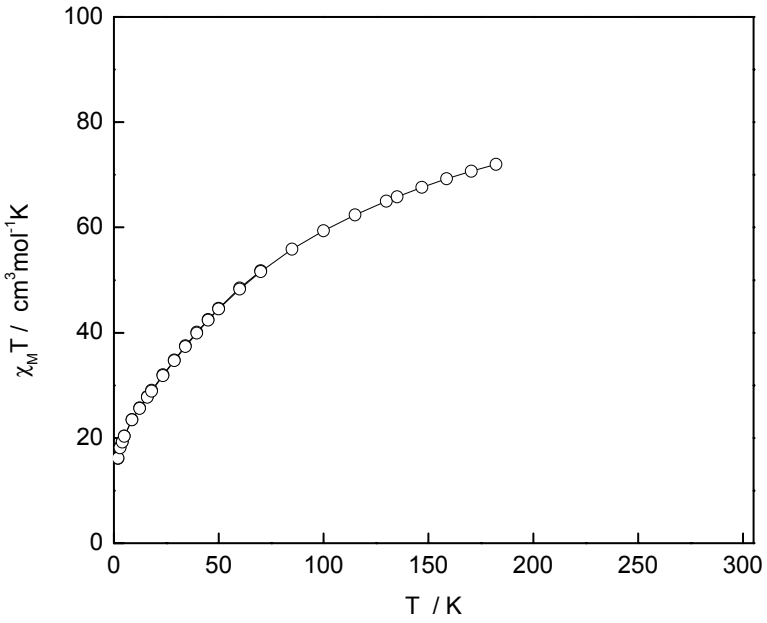

Fig. S3. Plot of DC $\chi_M T$ *vs. T* for freshly prepared **1**, in fields of 0.1 T (200 – 2 K) and 0.01 T (70 – 2 K); the solid line just joins the points. (new sample 2)

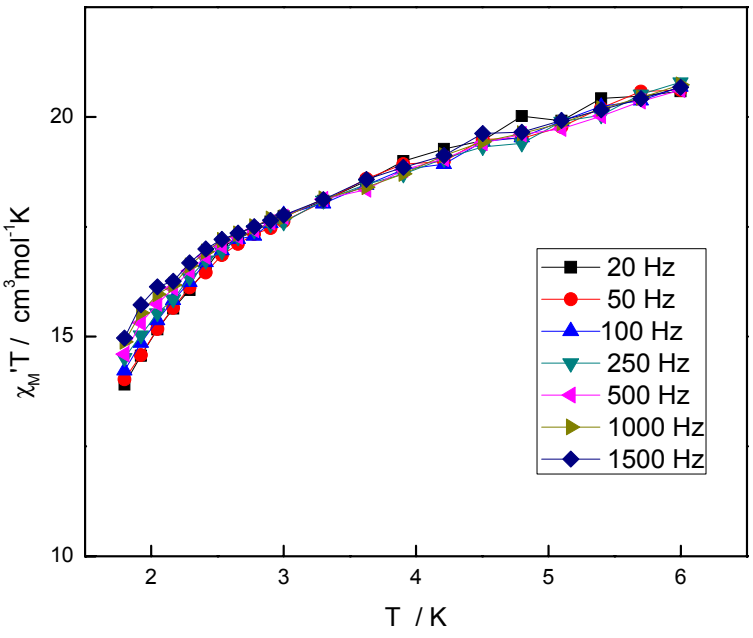

Fig. S4. Plot of AC $\chi_M'T$ *vs. T* for freshly prepared **1**. (new sample 2)

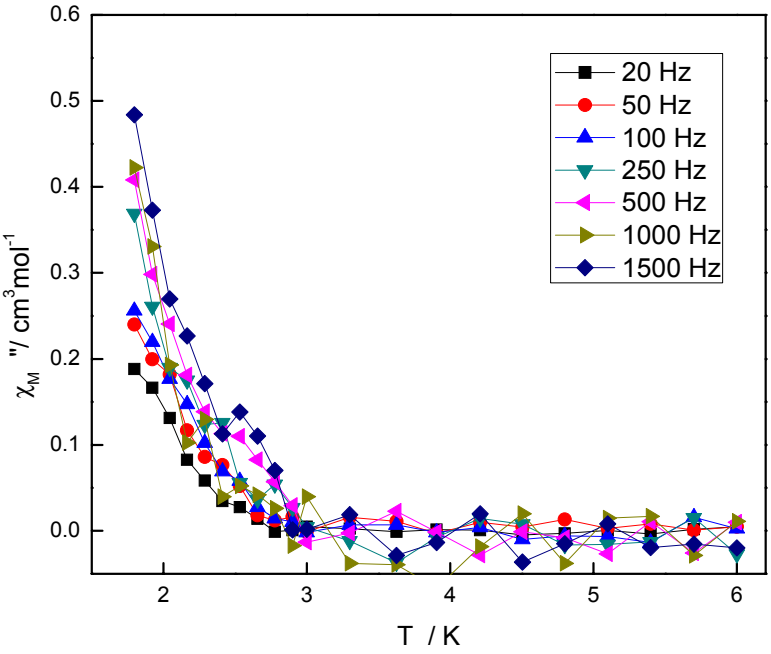

Fig. S5. Plot of AC χ_M'' vs. T for freshly prepared **1**. (new sample 2)

- **Plots of AC $\chi_M'T$ *vs.* *T* and χ_M'' vs. *T* data for 1 in applied DC fields**

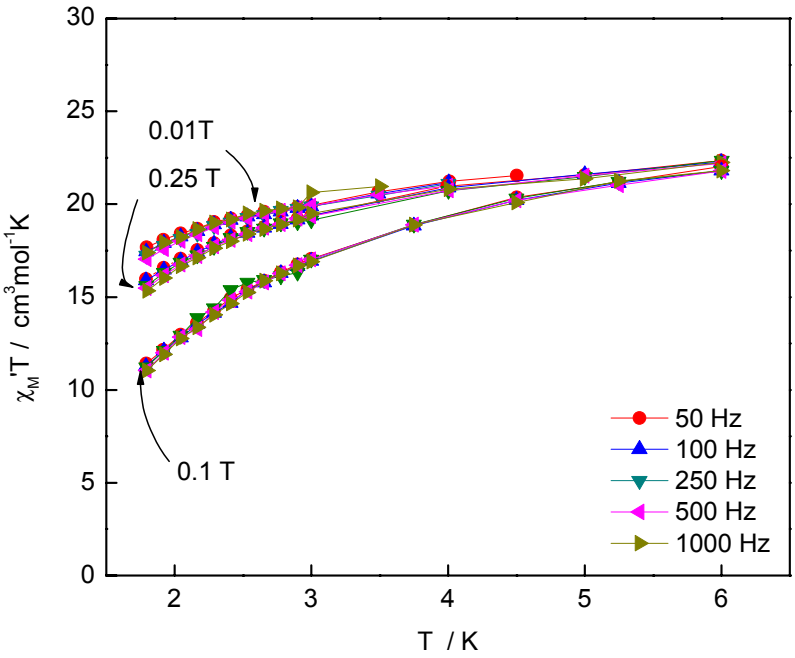

Fig. S6 Plots of AC $\chi_M'T$ *vs.* *T* data for **1** (new sample 3) at the frequencies shown in DC fields of 0.01, 0.1 and 0.25 T

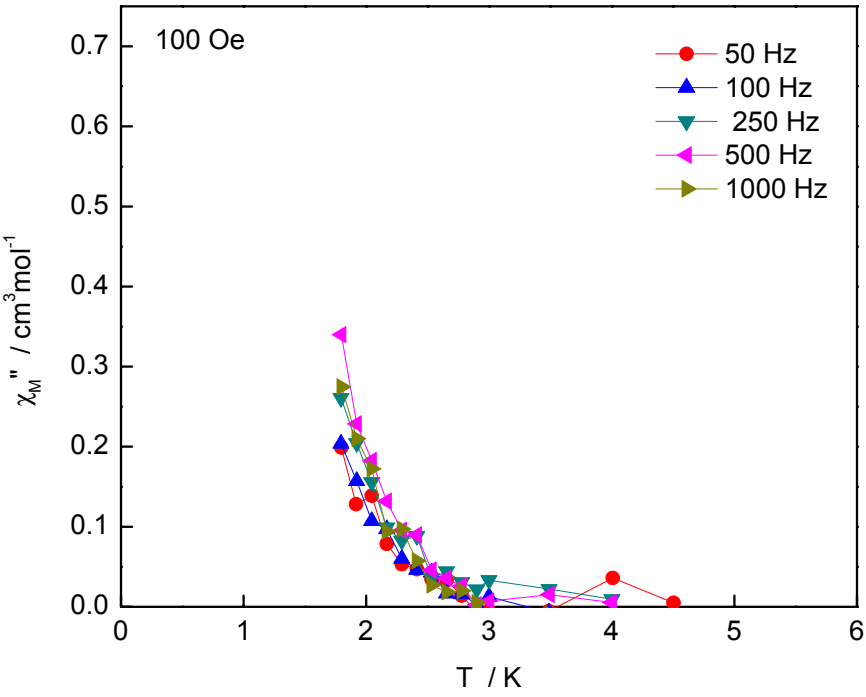

Fig. S7 Plots of AC χ_M'' vs. T for freshly prepared **1**. (new sample 3) in a DC field of 100 Oe (0.01 T).

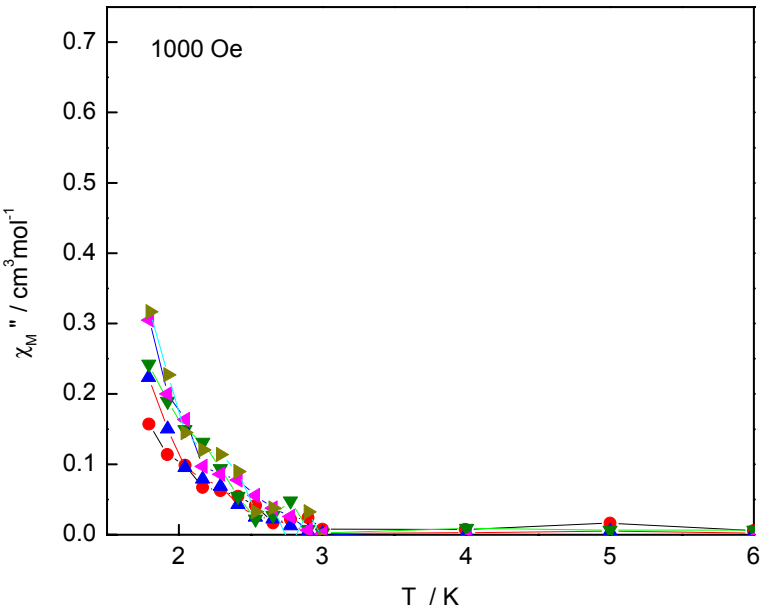

Fig. S8 Plots of AC χ_M'' vs. T for freshly prepared **1**. (new sample 3) in a DC field of 1000 Oe (0.1T). See Fig S7 for colour code for frequencies.

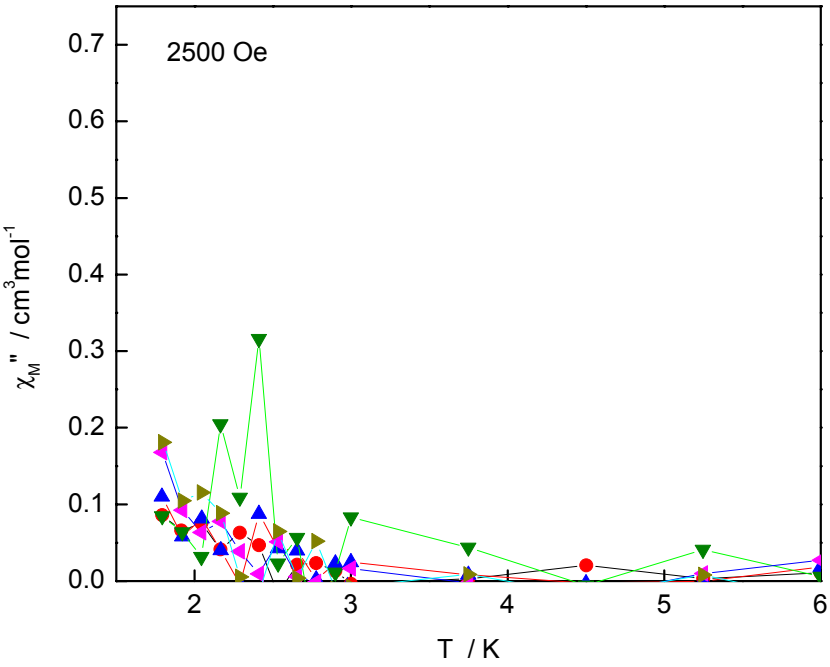

Fig. S9 Plots of AC χ_M'' vs. T for freshly prepared **1**. (new sample 3) in a DC field of 2500 Oe (0.25 T). See Fig S7 for colour code for frequencies. There is large scatter in this DC field.

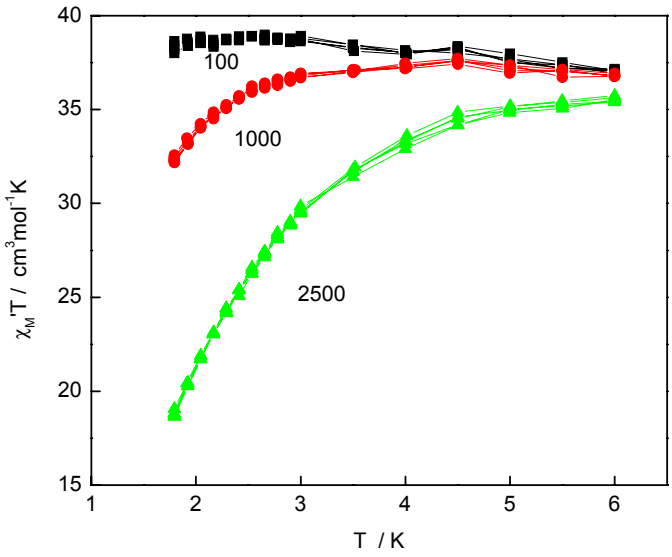

Fig. S10 Plots of AC $\chi_M'T$ *vs. T* data for **1** (new sample 1 **aged** in the Squid sample holder for 1 week) in DC fields of 100, 1000, 2500 Oe.

Thermal stability of 1 including TGA.

The TGA for a freshly prepared 18 mg crystalline sample of 'new sample 1', for which the unit cell was checked, is given in Fig S11. There is only a small decrease in mass between 20 to 50 °C indicative of thermal stability at room temperature, at least over short time frames. The expected % mass loss for loss of $5CH_2Cl_2$ is 7.76% and there is a hint of a corresponding inflection in the TGA at ~80 °C. The plateau in mass

loss just above 100 °C is indicative of a 15% mass loss meaning that thermal decomposition within the Mn_{32} complex is occurring. We note that TGA data for another large $Mn^{III}_{12}Mn^{II}_{9}$ aggregate, isolated as a $7.5H_2O$ hydrate,[1] showed a plateau in the TGA corresponding to 6.41% mass loss (see ESI; not assigned[1]) , at 150 °C, compared to a calculated loss of 4.05% for complete dehydration. Thus, it seems such TGA behaviour is not uncommon in these large Mn_x complexes. The magnetism in that study was done using a sample wet with mother liquor to prevent solvate loss. In previous work on a Mn_{16}–carboxylate complex,[2] we recognised the extreme thermal and hydrolytic instability, and the rapid effects this had on magnetic behaviour, and no such behaviour is evident in **freshly** prepared samples of complex **1**. In summary, we are confident that the magnetism reported here is intrinsic to **1** and not to a combination of **1** and some partially desolvated form of **1** or traces of another byproduct.

Importantly, we have noted that repeating magnetic measurements on a sample of **1** that has stood for a few days in the sample holder, in the lab., leads to higher $\chi_M T$ (DC) and $\chi_M' T$ (AC in-phase) than do the fresh samples, and this is probably the source of the higher values, that showed differences between DC and AC values at low temperatures, given in the first version of the paper. See also Fig S10.

1. S. Nayak, Y. Lan, R. Clérac, C. E. Anson, A. K. Powell, *Chem. Commun.* 2008, 5698-5700

2. D.J. Price, S.R. Batten, B. Moubaraki, K.S. Murray, *Chem. Commun.,* 2002, 762-763

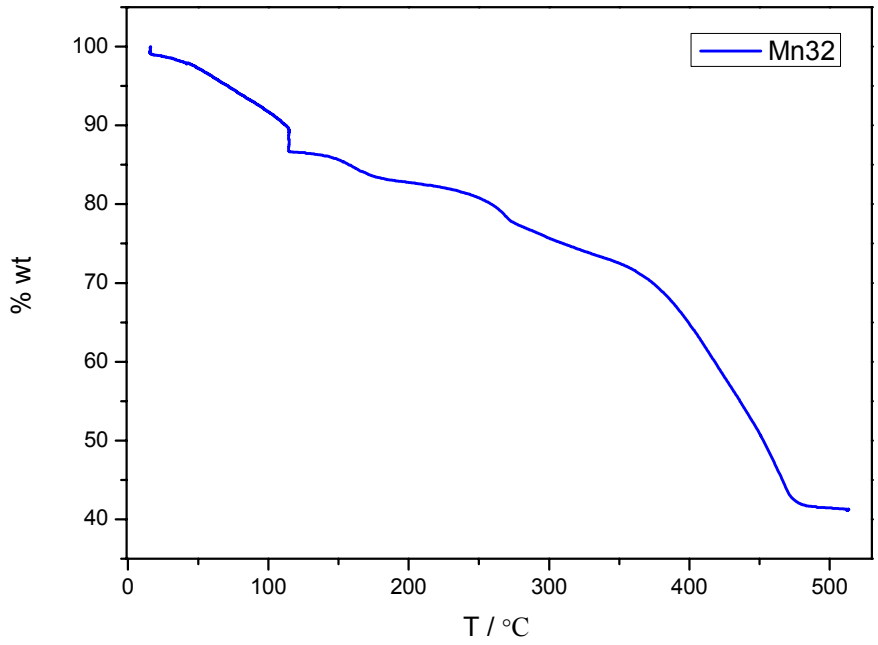

Fig. S11 TGA plot for freshly prepared sample of **1**. The rapid drop at 100 °C is an instrumental artefact due to changing the temperature ramp rate to a higher value above 100 °C